Supporting Information

Mechano-Bactericidal Titanium Surfaces for Bone Tissue Engineering

Tristan Le Clainche[1], Denver Linklater[1], Sherman Wong, Phuc Le, Saulius Juodkazis, Xavier Le Guével, Jean-Luc Coll, Elena P. Ivanova[*], Véronique Martel-Frachet[*]

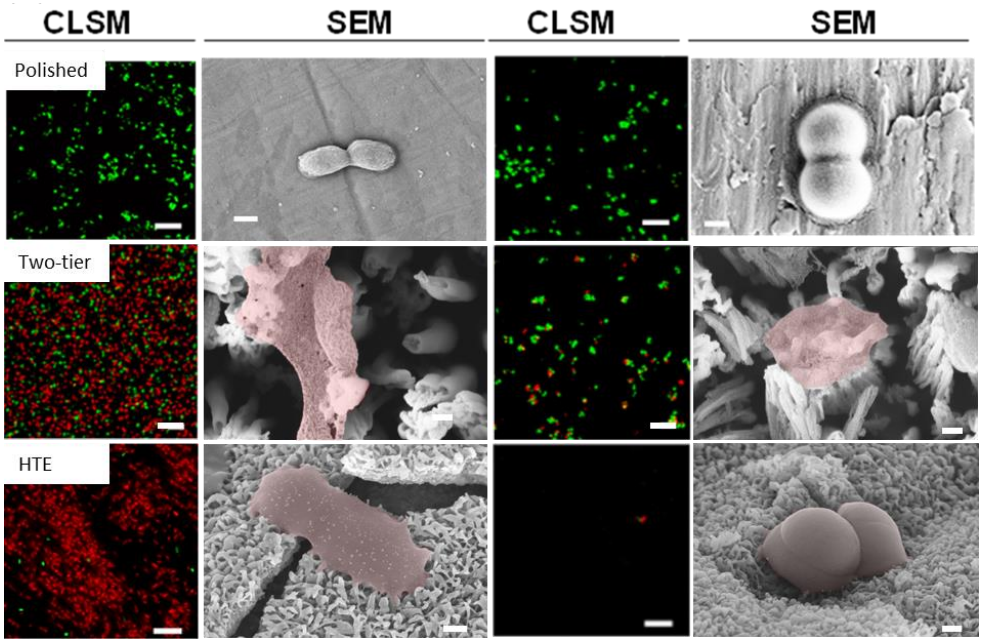

Figure S1. Antibacterial activity of polished, two-tier and HTE Ti surfaces towards *Pseudomonas aeruginosa* and *Staphylococcus aureus*, represented by CLSM and SEM images, respectively. CLSM scale bars are 10 µm, SEM scale bars are 200 nm.

Table S1. Assessment of bactericidal properties of nanostructured Ti surfaces.

	Pseudomonas aeruginosa		***Staphylococcus aureus***	
Sample	Antibacterial activity (% non-viable cells)	Cell Attachment ($x10^3$) cells/mm^2	Antibacterial activity (% non-viable cells)	Cell Attachment ($x10^3$) cells/mm^2
Polished	4.7 ± 3.9	63.4 ± 21.4	8.8 ± 6.5	19.8 ± 7.0
Two-tier	87 ± 2	270.3 ± 20	72.5 ± 13	2.1 ± 0.5
HTE	98.8 ± 0.7	230.8 ± 38.3	87.4 ± 10.2	2.2 ± 0.8

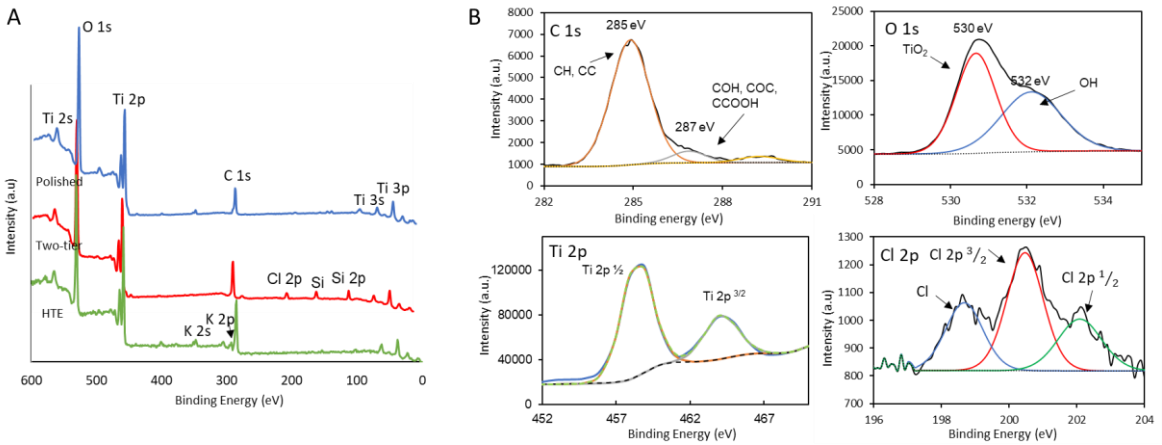

Figure S2. Surface chemical characterization of modified and polished Ti surfaces. (A) Wide survey spectra of polished, two-tier and HTE Ti. (B) Narrow spectral window scans of C 1s, O 1s, Ti 2p and Cl 2p bands.

Table S2. Characterization of surface physico-chemical characteristics

Surface Geometric Parameters			
	Polished	Two-Tier	HTE
Etch	0	40 min	6 h
Pitch (nm)	-	1729 ± 621	-
Cap/edge width (nm)	-	158 ± 40	10
Pillar/Edge Density	-	6.69 ± 1.4 (pillar/μm^2)	20 ± 13 (edge/μm^2)
Pillar Height/Edge Length	-	3.5 ± 0.5 µm	8.0 ± 1.8 ($\mu m/\mu m^2$)
Wettability			
Water contact angle (°)	60.1 ± 8.0	98.4 ± 5.8	22.00 ± 2.2
Elemental Composition (At%)			
O	34.275 ± 1.33	29.945 ± 0.33	56.65 ± 1.24
C	19.25 ± 0.31	26.605 ± 0.33	13.5 ± 0.25
Ti	32.98 ± 7.7	29.27 ± 2.52	22.65 ± 3.5
Cl	-	1.075 ± 0.05	-
K	-		7.25 ± 0.11

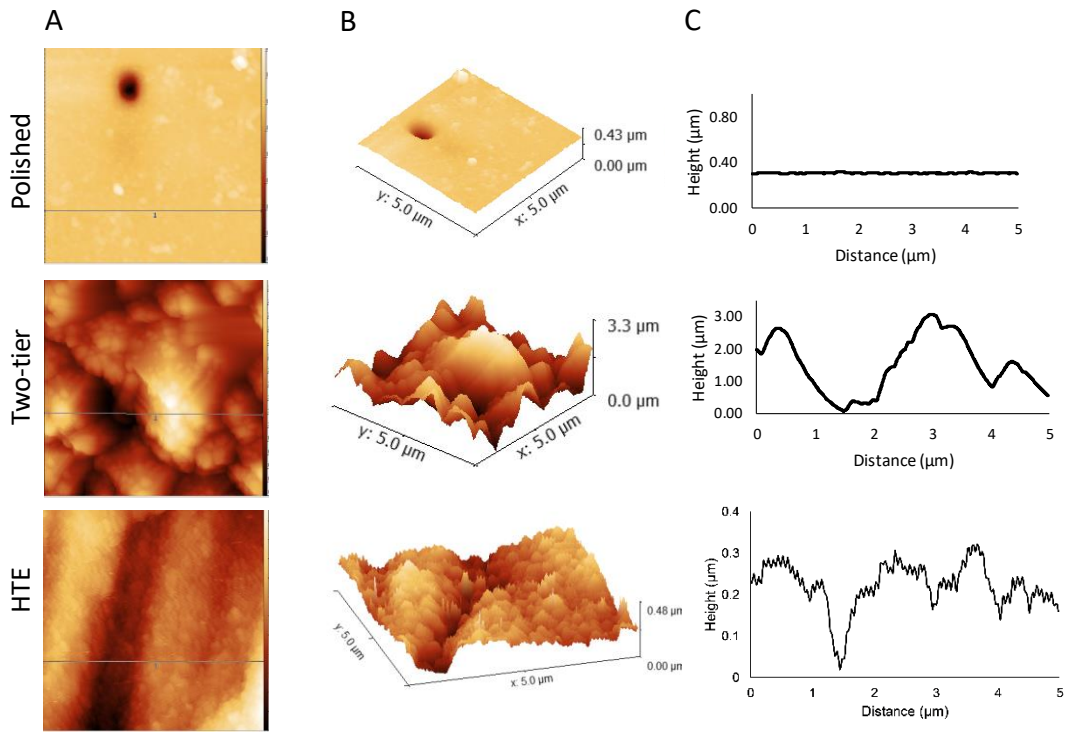

Figure S3. Surface roughness analysis of polished, Two-tier and HTE surfaces. Representative height scans (A) 3D reconstructions of height scans (B) and line scans (C) of respective Ti surfaces over a 5 × 5 µm scan area.

Table S3. AFM surface roughness analysis of polished, Two-tier and HTE Ti surfaces.

Surface Roughness			
Sample name	**Polished**	**Two-tier**	**HTE**
S_{max} (nm)	19 ± 3	3956 ± 864	581.3 ± 142.1
Median Height (nm)	17 ± 2	1511 ± 317	385.1 ± 110.9
Mean roughness R_a (S_a)	2.5 ± 0.3	446.3 ± 12	92.1 ± 36.5
Root mean square height R_{ms} (S_q)	3 ± 0.3	567 ± 11	109.9 ± 44.8
Skewness	- 0.05 ± 0.1	0.42 ± 0.1	-0.4 ± 0.2
Kurtosis	3.41 ± 0.7	0.305 ± 0.02	-0.5 ± 0.3

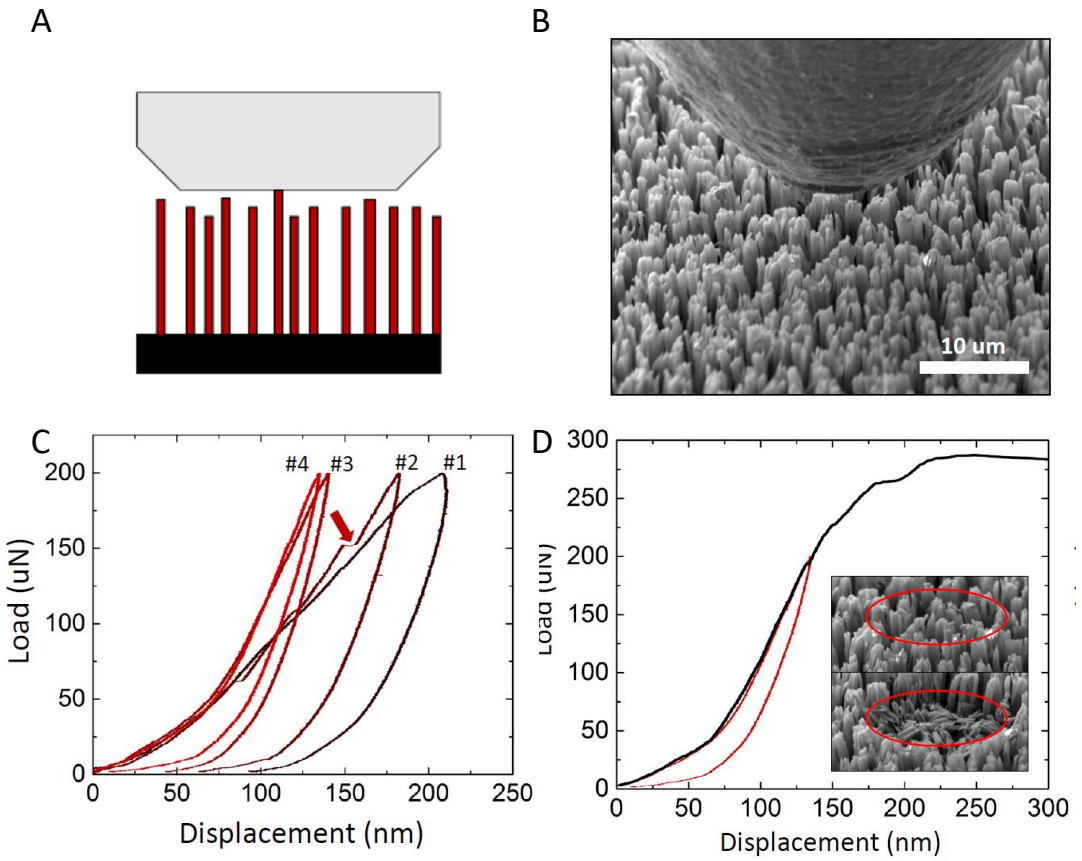

Figure S4. a) Schematic representation of the tip engaging the non-uniform surface the Ti micropillar array. b) SEM image of the tip over the Ti nanostructures, taken at a tilt of 60°. c) Multiple 200 μN load indents on the same region. d) Stress/strain curves (black) obtained from the sample after a consistent tip-to-sample engagement was achieved. The last elastic indent (red) is also included to show that prior to plastic deformation the sample behaviour is identical to previous indents. Inset SEM images shows the sample before and after plastic deformation.

Supplementary Results:

Surface Chemical Characterization: Analysis of the surface chemical composition confirmed the Ti nanostructures to be titanium dioxide (TiO_2), as indicated by the characteristic Ti 2p doublet peaks in the wide scan XPS survey and high concentrations of surface oxygen (Figure S3)**.** There were no changes to the crystalline Ti phase following prolonged periods of either plasma or hydrothermal etching, as confirmed by XRD analysis of the surface crystallinity (Figure 1).

The polished Ti possessed a water contact angle (WCA) of 60°. Nanostructuring of the bulk Ti by hydrothermal etching caused an increase in the wettability of the surfaces (Table 1) with a WCA of just 22°. In contrast, the formation of TiO_2 pillar arrays *via* plasma etching caused an increase in hydrophobicity (WCA 98°) (Table 1). This is most likely a result of the increasing surface roughness with increasing etch time, which results in the ability of the surface to entrap air between the features.

Nanoindentation: As expected from the variable Ti pillar height, the first indent few indents made were not very informative. Mechanical healing, where cyclic indentation to very low loads is performed on the sample, was used to create a more ideal surface for nanoindentation. Low loads will result in elastic deformation (no change) to the majority of the sample. However, defects act as focal points for stress. Therefore, even low loads will allow enough stress for those defects to be removed from the sample, which creates a more ideal surface for subsequent indentation. Here, this technique allows the tip to engage all the Ti pillars at roughly the same time. In Figure S4C, the curves are starting to look a lot more consistent with what we expect. There are “pop-in” events during the loading segment of indent #2, which are indicated by the arrow. This is indicative of a NW that has bent slightly at that point. After this occurs the

load/unload curves become quite consistent. In Figure S4D, the curve doesn't begin with a linear region, which is expected from the elastic regime. Instead, it appears similar to pointed tip loading, which increases exponentially as the tip engages more of the sample. Most probably, the tip is engaging more NWs over this range. This suggests there is still a height difference (~60 nm) between the tallest and shortest NWs in the indented region. The slope of the elastic region can be used to measure an elastic modulus:

$$E_r = \frac{\sigma}{\varepsilon} = \frac{F/A}{\Delta L/L_0}$$

Where E_r is elastic modulus, σ is stress, ε is strain, F is load force (y-axis on the plot), A is contact area, ΔL is displacement (x-axis of plot), and L_0 is pillar height. Rearrange for F as a function of ΔL gives:

$$F = \left(E_r \frac{A}{L_0}\right) \Delta L$$

Here, we calculated a value of ~100 GPa (using a very rough estimate for contact area) which is similar to that of bulk Ti. The onset of plasticity (where the curve goes from linear to curved) occurs at ~150 nm, while fracture (where the curve goes flat) occurs at ~225 nm. For a NW of ~4 um length that is ~4% and ~6%, respectively. These values will vary based on the NW height and material. As we are now engaging all the NWs within the indented region at the same time, a fracture event in the curve results in all the NWs bending at the same time.